Real-time compaction of nanoconfined DNA by an intrinsically disordered macromolecular counterion

Citation for the original published paper (version of record):
Sharma, R., Kesarimangalam, S., Holmstrom, E. et al (2020). Real-time compaction of nanoconfined DNA by an intrinsically disordered macromolecular
counterion. Biochemical and Biophysical Research Communications, 533(1): 175-180.
http://dx.doi.org/10.1016/j.bbrc.2020.06.051

Biochemical and Biophysical Research Communications 533 (2020) 175–180

Contents lists available at ScienceDirect

Biochemical and Biophysical Research Communications

journal homepage: www.elsevier.com/locate/ybbrc

Real-time compaction of nanoconfined DNA by an intrinsically disordered macromolecular counterion

Rajhans Sharma [a], Sriram KK [a], Erik D. Holmstrom [b, c, **], Fredrik Westerlund [a, *]

[a] Department of Biology and Biological Engineering, Chalmers University of Technology, Gothenburg, Sweden
[b] Department of Molecular Biosciences, University of Kansas, Lawrence, KS, USA
[c] Department of Chemistry, University of Kansas, Lawrence, KS, USA

ARTICLE INFO

Article history:
Received 27 May 2020
Accepted 10 June 2020
Available online 18 September 2020

Keywords:
Nanofluidic device
Protein-DNA interaction
Hepatitis C virus core protein
Macromolecular counterion
Intrinsically disordered protein
DNA condensation and compaction

ABSTRACT

We demonstrate how a recently developed nanofluidic device can be used to study protein-induced compaction of genome-length DNA freely suspended in solution. The protein we use in this study is the hepatitis C virus core protein (HCVcp), which is a positively charged, intrinsically disordered protein. Using nanofluidic devices in combination with fluorescence microscopy, we observe that protein-induced compaction preferentially begins at the ends of linear DNA. This observation would be difficult to make with many other single-molecule techniques, which generally require the DNA ends to be anchored to a substrate. We also demonstrate that this protein-induced compaction is reversible and can be dynamically modulated by exposing the confined DNA molecules to solutions containing either HCVcp (to promote compaction) or Proteinase K (to disassemble the compact nucleo-protein complex). Although the natural binding partner for HCVcp is genomic viral RNA, the general biophysical principles governing protein-induced compaction of DNA are likely relevant for a broad range of nucleic acid-binding proteins and their targets.

1. Introduction

Single-molecule methods have revolutionized our understanding of nucleic acid-protein interactions. By manipulating and visualizing single biomolecules, detailed information that would be hidden in ensemble methods can be obtained. Single-molecule approaches for studying genome-length (>10 kbp) double-stranded DNA (dsDNA) include optical [1] and magnetic [2] tweezers, as well as DNA curtains [3]. One main drawback with these techniques is that they rely on anchoring at least one DNA end to a fixed substrate. This can be a substantial experimental limitation since many important biomolecular reactions occur at the ends of dsDNA (e.g., repair of double-stranded breaks and elongation of telomeric repeats). Thus, there is a strong need for single-molecule methods that allow both ends of long dsDNA molecules to be studied in real time.

Nanofluidic channels have emerged as useful tools for studying individual DNA molecules [4] and DNA-protein complexes [5]. The channels spatially confine long biopolymers in solution and force them to align along the channels. Importantly, this approach leaves the ends of the DNA unmodified, enabling single-molecules studies of biomolecular reactions that preferentially occur at the termini. To date, the vast majority of studies utilizing nanofluidic confinement have been carried out under static solution conditions where the samples were equilibrated outside the device and then visualized inside the nanochannels. In 2013, Zhang et al. introduced a nanofluidic design where a solute of interest (e.g., DNA-binding protein) is allowed to *passively* diffuse into the nanochannels, making it possible to visualize biomolecular interactions in real time [6]. We recently extended this solution-exchange principle by designing a dynamic nanofluidic device where the solution surrounding the confined DNA can be *actively* exchanged [7]. Compared to a traditional nanofluidic device (Fig. 1a), our novel dynamic device (Fig. 1b) has a “reaction chamber” at the center of every nanochannel. These reaction chambers have slightly larger dimensions than the nanochannels leading into and out of them (Fig. 1c). In this way, a single DNA molecule can be “entropically trapped” inside each reaction chamber. The solution conditions are then varied using a very shallow slit that runs orthogonally across

* Corresponding author. Department of Biology and Biological Engineering, Chalmers University of Technology, Gothenburg, Sweden.
** Corresponding author. Department of Molecular Biosciences and Department of Chemistry, University of Kansas, Lawrence, KS, USA.
E-mail addresses: erik.d.holmstrom@ku.edu (E.D. Holmstrom), fredrik.westerlund@chalmers.se (F. Westerlund).

https://doi.org/10.1016/j.bbrc.2020.06.051

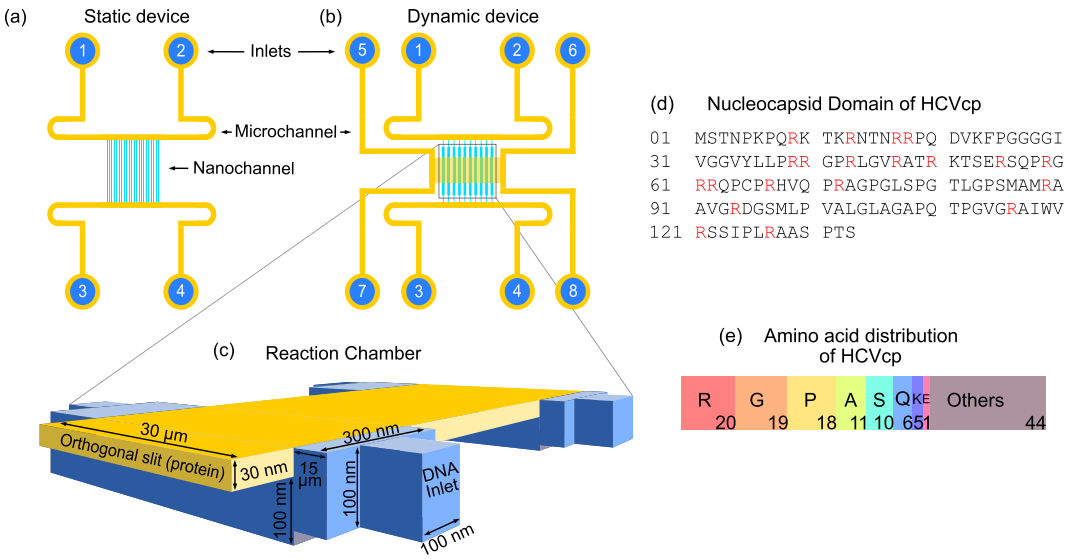

Fig. 1. Nanofluidic device and HCVcp. Schematics of (a) the static and (b) the dynamic nanofluidic devices, the latter of which entropically traps single DNA molecules in a specially designed (c) reaction chamber. The amino acid sequence of (d) the nucleocapsid domain of HCVcp and (e) a graphical representation of the relative abundance of each amino acid.

the reaction chambers (Fig. 1c). Importantly, the slit is too thin for the extended DNA to pass through. In a previous study, we demonstrated the functionality of this device by exposing confined DNA molecules to various solutes like spermidine and DNAse 1, where the latter allowed us to visualize nuclease activity on single DNA molecules in real time.

In this report, we demonstrate, for the first time, how the dynamic nanofluidic device facilitates real-time observations of protein-induced conformational changes in individually confined DNA molecules. The protein we study is the intrinsically disordered, positively charged nucleocapsid domain of the hepatitis C virus core protein (HCVcp). HCVcp plays an important role in viral assembly by compacting all ~10^4 nucleotides (nts) of the viral genome into a 30–50 nm nucleocapsid particle [8]. Although the hepatitis C virus has a single-stranded RNA (ssRNA) genome, the HCVcp can also form nucleocapsid-like particles in the presence of dsDNA [9]. Furthermore, HCVcp functions as a promiscuous nucleic acid chaperone and helps short (<100 nts) structured DNA and RNA molecules to adopt compact (e.g., folded) conformations [8]. Inspired by the multiple nucleic acid binding properties of HCVcp, we set out to determine if it can compact genome-length dsDNA. Using nanofluidic devices, we show that low-micromolar concentrations of HCVcp can efficiently compact dsDNA. Intriguingly, all compaction events start at the ends of linear DNA, suggesting that HCVcp prefers to interact with these regions of the duplex. Furthermore, we show that compaction is reversible by iteratively exposing the dsDNA to either HCVcp (to promote compaction) or Proteinase K (to disassemble the compact nucleoprotein complex). Finally, we demonstrate that HCVcp can bridge nearby segments of dsDNA during the compaction process.

2. Materials and Methods

2.1. Nanofluidic device

Channels in the static nanofluidic device are 100 nm deep, 150 nm wide, 500 μm long and fabricated in oxidized silicon as described elsewhere [4] (Fig. 1a). Fabrication of the dynamic nanofluidic device is also described in detail elsewhere [7]. Briefly, the nanochannels are 100 nm wide and 100 nm deep except for the 60 μm long central region in each channel, herein referred to as the reaction chamber, that has a width of 300 nm and a depth of 130 nm. A 500 μm long slit runs orthogonally across the nanochannels with a depth of 30 nm and a width of 30 μm. A schematic layout of the dynamic nanofluidic device is shown in Fig. 1b–c.

To prevent sticking of the protein to the channel walls, the nanofluidic devices were coated with a lipid bilayer. The lipid membranes were prepared from 99% 1-palmitoyl-2- oleoyl-sn-glycero-3-phosphocholine (POPC, Avanti) and 1% N- (fluorescein-5-thiocarbamoyl)-1,2-dihexadecanoyl-sn-Glycero-3-phosphoethanolamine triethylammonium salt (fluorescein-DHPE, Invitrogen). The fluorescent DHPE ensures that the surfaces of the device remained coated for the duration of the measurement. The coating procedure is described in detail elsewhere [10].

2.2. Expression and purification of HCVcp

The nucleocapsid domain of the hepatitis C virus core protein (HCVcp) was recombinantly expressed and purified as described previously [11]. Briefly, a 6× histidine-tagged variant of the desired amino acid sequence (Fig. 1d) was codon optimized for *E. coli* and cloned into a pET-47b(+) vector, which was then transfected into BL21 (DE3) cells. After 3 h of growth at 37 °C in lysogeny broth, protein expression was induced with 500 μM isopropyl β-D-1-thiogalactopyranoside. After 3 h of induction, bacterial cells were pelleted, lysed in 6 M guanidinium chloride, and homogenized prior to protein purification via immobilized metal-ion affinity chromatography. The 6× histidine tag was cleaved off using 3C protease and further purified using high-performance liquid chromatography. Purified protein was lyophilized and then resuspended in 50 mM sodium phosphate (pH 7.0) with 40 mM KCl and stored at −20 °C until use.

2.3. Sample preparation

All experiments were carried out in 50 mM Tris-HCl buffer (Sigma-Aldrich) at pH 7 containing 50 mM NaCl and 0.5 mM EDTA. The dsDNA samples used were: bacteriophage T4-DNA (166 kbp, T4GT7 DNA, Nordic Biolabs), bacteriophage T7-DNA (39.9 kbp, Bioron GmbH), bacteriophage λ-DNA (48.5 kbp, Roche) and a circular DNA (cDNA) plasmid (133 kbp).

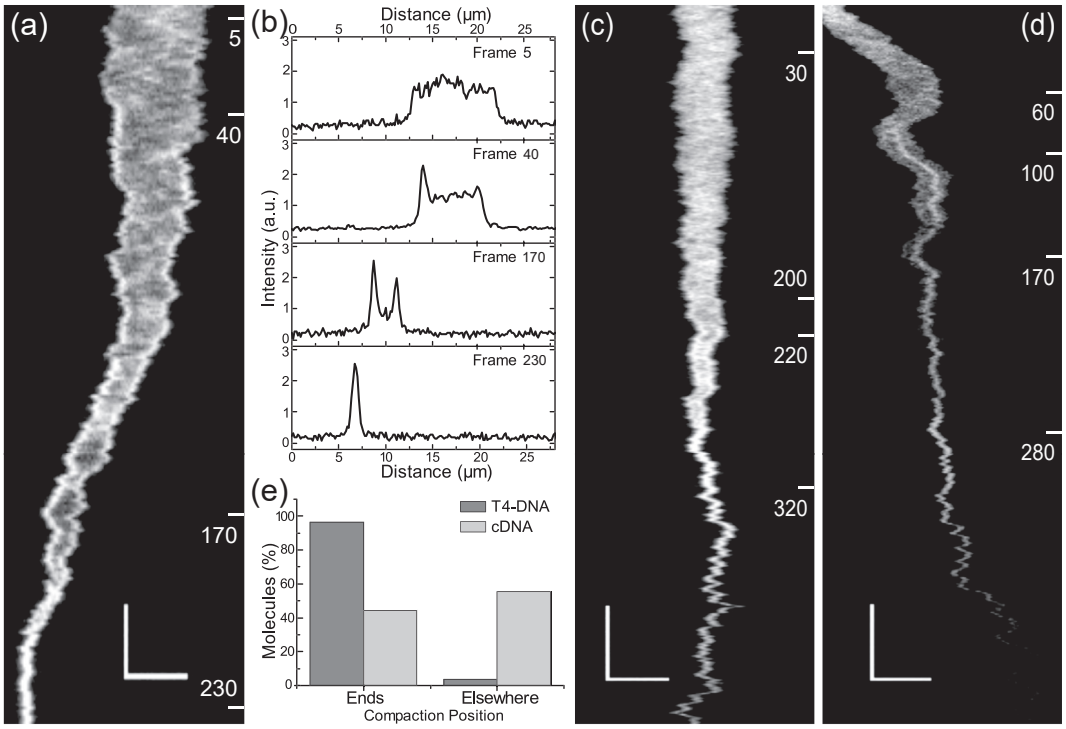

Fig. 2. Real-time observation of the interaction between HCVcp and genomic-length dsDNA in a dynamic nanofluidic device. (a) Kymograph showing that HCVcp (1.0 μM) initiates compaction of T4-DNA from both ends of the molecule (at 5 fps). (b) Spatial fluorescence intensity profiles from the kymograph in (a). Kymographs showing two different sites of compaction on separate cDNA molecules (at 9 fps): either at (c) the poles (ends) of the cDNA or (d) elsewhere. For (a,c,d) the scale bars represent 5 μm for the x-axis and 5 s for the y-axis. (e) Histogram depicting the percentage of T4-DNA (N = 66) and cDNA (N = 18) molecules having compaction events that begin at either the ends (poles) of the DNA or elsewhere.

The static nanofluidic device was used to visualize preformed protein-DNA complexes, which were prepared by mixing the desired ratio of DNA and protein and incubating for 1 h at room temperature. Subsequently, the DNA samples were fluorescently stained with YOYO-1 (Invitrogen) at a ratio of 25 base pairs to 1 dye and incubated for 15 min before use. Next, 10 μL of sample was loaded in one of the four inlets (Fig. 1a, Inlet 1–4) of the nanofluidic device, and the remaining three inlets were filled with buffer. Using pressure-driven flow, the DNA molecules were flushed through the microchannel to the front of the nanochannels and then pushed into the nanochannels by applying pressure to both inlets of the microchannel on one side of the nanochannels. The molecules are then allowed to equilibrate to for at least 30 s before imaging.

For the experiments in the dynamic nanofluidic device, we prepared two separate samples of DNA stained with YOYO-1 and protein. First, 10 μL of DNA sample was loaded in one of the four DNA inlets (Fig. 1b, Inlet 1–4), and the remaining three inlets were filled with buffer. Next, 10 μL of protein sample was loaded into one of the four additional inlets (Fig. 1b, Inlet 5–8) and the rest were filled with buffer. For the experiments involving Proteinase K (Invitrogen, AM2546), the HCVcp solution was loaded into inlet 5 or 6 and the Proteinase K solution was loaded into inlet 7 or 8. Using pressure-driven flow, the DNA molecules were flushed through the microchannel to the front of the nanochannels. Then, the DNA molecules were pushed through the nanochannels and into the reaction chambers (Fig. 1c) by applying pressure to both inlets on one side of the nanochannels. The molecules were then allowed to equilibrate for at least 30 s before the protein sample was introduced from the orthogonal slit using pressure-driven flow. Image acquisition began as soon as the protein was introduced into the reaction chamber. Once the DNA was fully compacted the flow of protein was stopped. For the Proteinase K experiments the flow was iteratively switched between the HCVcp-side of the slit and the Proteinase K side.

All imaging was done using a Zeiss AxioObserver.Z1 fluorescence microscope equipped with a Hamamatsu digital CMOS C11440–22CU camera, a 63× oil immersion TIRF objective (NA = 1.46) and a 1.6× optovar. We used the Zeiss filter set 44, which has an excitation band of 475 ± 40 nm and emission band of 530 ± 50 nm. Unless otherwise specified, the Zen pro software was used to capture a series of frames, each with an exposure of 100 ms, resulting in 9 frames per second. All data analysis was performed using ImageJ and/or custom-written MATLAB-based scripts.

3. Results

HCVcp is a multifunctional intrinsically disordered protein with a wide range of nucleic acids interactions [12,13]. HCVcp preferentially interacts with small (<100 nts) structural motifs excised from the viral genome resulting in the formation of nucleocapsid-like particles [11]. HCVcp can also chaperone several different nucleic acid conformational transitions, including the dimerization of a structured RNA element that is comprised of 98 nts and located at the 3′-end of the viral genome [8]. However, it is not well-known if/how HCVcp interacts with long dsDNA molecules that are more similar in length to the genomic RNA (~10^4 nts) contained within the nucleocapsid of the hepatitis C virus. Therefore, we set out to characterize the structural and dynamic aspects of the molecular interactions between HCVcp and genome-length dsDNA.

3.1. HCVcp initiates compaction of linear dsDNA from the ends

To monitor the real-time compaction of linear T4-DNA by HCVcp, we use the dynamic nanofluidic device (Fig. 1b, Materials

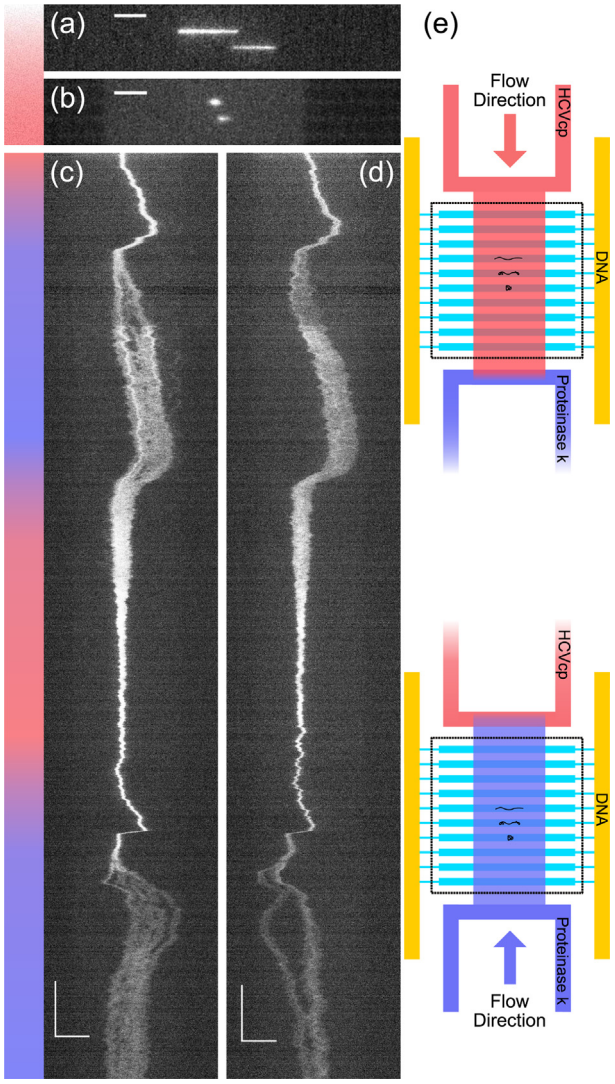

Fig. 3. Iterative compaction of genome length dsDNA-HCVcp complexes. The compaction of YOYO-1 stained T4-DNA was induced by the addition of HCVcp (red). Disassembly of the nucleoprotein complex was induced by the addition of Proteinase K (blue). Images of (a) two extended molecules, each confined within a reaction chamber, and (b) their compact form during continuous flow of HCVcp from the shallow orthogonal slit. For (a,b) the scale bar is 5 μm. The initial compaction was not imaged to prevent photobleaching of YOYO-1. Images are used to construct (c,d) kymographs showing the subsequent disassembly of the compact nucleoprotein complexes by introducing Proteinase K into the reaction chamber from the other side of the shallow slit, which marks the beginning of the iterative cycle of dissassembly and compaction. For (c,d) the x-axis scale bar is 10 μm and the y-axis scale bar is 20 s. (e) Schematic diagram of the flow directions used to compact and disassemble the HCVcp nucleoprotein complexes.

and Methods). Solutions with various concentrations of HCVcp (i.e., 0.0, 0.5, 1.0, 1.5 μM) were continuously flushed across the reaction chambers containing single confined dsDNA molecules via the orthogonal slit. Since the protein was not labeled, we relied on changes in YOYO-1 emission to monitor the action of the protein. We verified that the fluorescence intensity of YOYO-1 remained constant during the introduction of HCVcp, indicating that protein binding and the resulting DNA compaction did not displace the intercalated dyes (Fig. S1).

When flushing the reaction chambers with solutions containing 1.0 μM HCVcp, we observed a gradual decrease in the extension of T4-DNA molecules (Fig. 2a and Fig. S2a,b) over the course of ~50 s. Compaction of the DNA was evident based on both a sudden decrease in the total length of the DNA and a local increase in the YOYO-1 emission intensity along the DNA (Fig. 2b). The kymograph in Fig. 2a shows the appearance of such a compaction event at the left end of the molecule ~8 s after the introduction of HCVcp (Fig. 2a and b; frame 40) and again on the right side of the molecule a few seconds later (Fig. 2a; frame 60). Interestingly, after analyzing the kymographs of 66 individual DNA molecules, we observed that all but one molecule began to compact from the ends of the DNA (Fig. 2e). This strongly suggests that the mechanism for HCVcp-induced compaction involves the ends of linear DNA. We stress that this phenomenon would be very difficult to study with single DNA molecule techniques that rely on anchoring the DNA at the ends.

At higher concentrations of HCVcp (e.g., 1.5 μM), the rate of DNA compaction increased (Fig. S2c). Conversely, at lower protein concentrations (e.g., 0.5 μM), both the rate of compaction and extent of compaction decreased. Together, these observations highlight the pronounced concentration dependence of end-initiated protein-induced compaction of DNA by HCVcp.

Two possible reasons for end-initiated compaction are: (*i*) the protein preferentially accumulates at the ends of the DNA and/or (*ii*) the geometry of the nanochannel favors compaction from the ends. To further explore these possibilities, we investigated the interaction between HCVcp and circular DNA (cDNA), which has no well-defined ends. cDNA is notoriously difficult to study with single-molecule methods since no ends are available for chemical modifications that permit anchoring of the DNA to an immobilized substrate. However, we have demonstrated in previous studies that nanochannels are perfectly suited for analysing single cDNA molecules [14–16].

Two kymographs depicting HCVcp-induced compaction of cDNA are shown in Fig. 2c–d (additional examples in Fig. S3). In contrast to linear T4-DNA, the compaction of cDNA was initiated at locations throughout the confined DNA. For seven of the 18 molecules observed, compaction was initiated at the “poles” of the extended cDNA. For the remaining 11 molecules, compaction began elsewhere (Fig. 2e). This observation indicates that HCVcp does not require ends to compact duplex DNA, even though initiation of compaction tends to occur at the ends when they are present.

3.2. Reversible compaction of dsDNA by HCVcp

To further demonstrate the utility of the nanofluidic device for investigating nucleoprotein interactions, we repeatedly compacted the same DNA molecule by iteratively flushing the reaction chambers with either HCVcp (to initiate compaction) or Proteinase K (to disassemble the nucleoprotein complex). This was accomplished by introducing HCVcp from one end of the orthogonal slit and subsequently introducing Proteinase K from the opposite end of the slit. Kymographs from two experiments where we followed the reversible compaction of dsDNA in real time are shown in Fig. 3. First, we flushed the reaction chambers with a solution containing 1.0 μM HCVcp to compact the T4-DNA (Fig. 3a and b red region). Then, we exchanged the solutions and introduced Proteinase K (6.9 μM) into the reaction chamber (Fig. 3c and d blue region). As Proteinase K digested the HCVcp, certain regions of compact DNA persist longer than others; although the DNA eventually returns to an extended conformation like that observed prior to compaction. The process could be repeated for the same DNA molecule, resulting in a similar response. An interesting observation in the kymographs in Fig. 3c and d is that the T4-DNA broke into smaller fragments. However, this did not ruin the cyclical experiment since the fragments were confined within the reaction chamber. Importantly, when the HCVcp was re-introduced into this reaction chamber, these fragments eventually ended up in the same compact nucleoprotein complex, which suggests that the protein

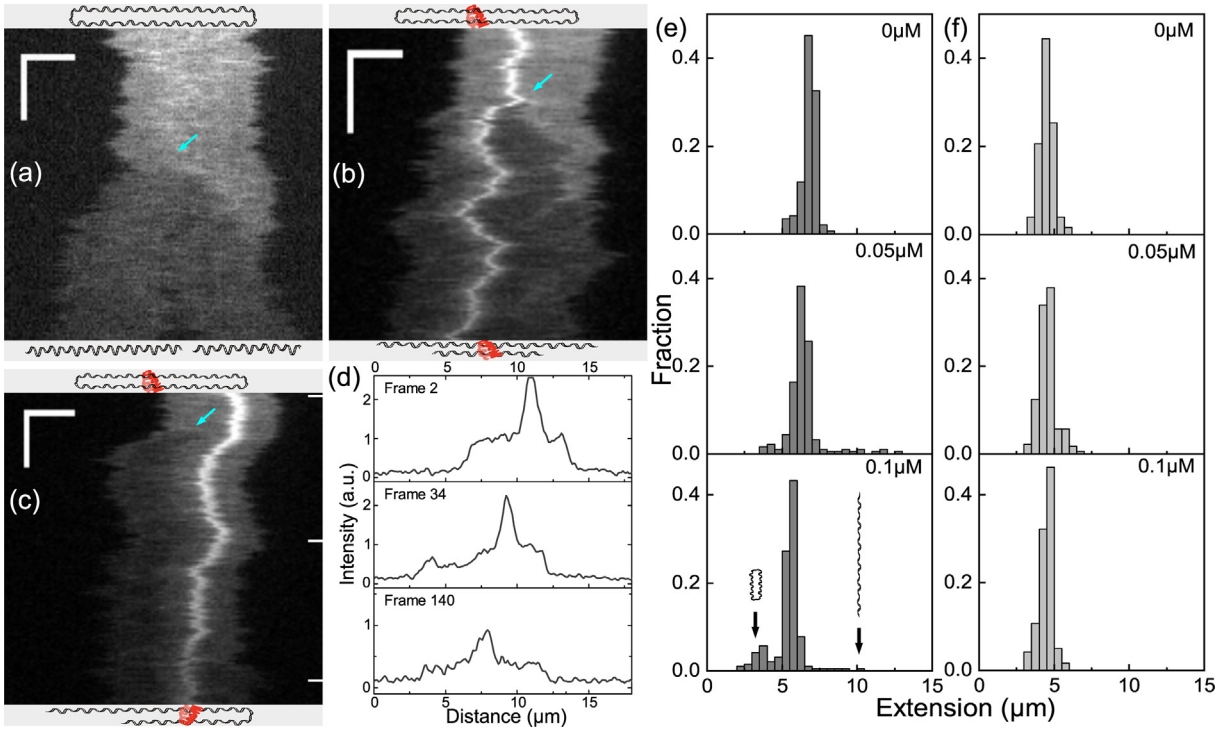

Fig. 4. Kymographs of cDNA cleavage in the (a) absence and (b,c) presence of HCVcp. Sketches of cDNA molecules before and after photoinduced double-stranded breaks are shown above/below each kymograph to illustrate the transition to the extended conformations. The concentration of HCVcp (red) in (b) and (c) is 1 μM and the concentration of circular DNA (black) is 5 μM base pairs. Scale bars for the x- and y-axes are 3 μm and 3 s, respectively. Histograms depicting the distribution of extensions for individual (e) λ-DNA or (f) T7-DNA molecules at different concentrations of HCVcp, where the dsDNA concentration is 5 μM base pairs. The arrows point out circular complexes and complexes consisting of two λ-DNA molecules, respectively. (For interpretation of the references to colour in this figure legend, the reader is referred to the Web version of this article.)

can bridge multiple fragments and incorporate them into the same nucleoprotein complex.

3.3. HCVcp can bridge adjacent DNA segments

To further investigate the local compaction of cDNA, we used a traditional *static* nanofluidic device (Fig. 1**a**), which has narrower channels (width = 100 nm, height = 150 nm) than those associated with the reaction chambers of the dynamic nanofluidic device. The main advantage with the traditional static nanofluidic device is that the enhanced confinement from the narrower channels results in more extended DNA molecules. Similar to our experiments in the dynamic nanofluidic device, we observed that compaction could be initiated anywhere along the cDNA. Next, we wanted to determine if the local compaction is restricted to one segment of the cDNA, or if HCVcp-induced compaction can bridge adjacent segments of the same cDNA. To address this question, we created random double-stranded breaks in the confined cDNA by exposing the YOYO-1 fluorophores to high-intensity excitation light [17]. When a double-stranded break was formed in the absence of HCVcp (Fig. 4a), the broken cDNA began to uncoil and adopt extended linear conformations that were aligned with the nanochannels [15]. After one (Fig. 4b) or more (Fig. 4c) break events in the presence of HCVcp, the newly formed linear DNA molecules also aligned along the nanochannel. However, the compact regions of DNA remained in place, held together via HCVcp. This suggests that the sites of compaction can bridge adjacent segments from the same cDNA and/or fragments from different DNA molecules. This is in qualitative agreement with the data presented in Fig. 3 where we observed that more than one dsDNA fragment can be incorporated into a single compact nucleoprotein complex.

3.4. Nucleic acid chaperoning activity of HCVcp

Thus far we have demonstrated that the positively charged HCVcp can function as a macromolecular counterion that associates with and compacts genome-length dsDNA. However, it is also known that HCVcp can function as a potent nucleic acid chaperone for short structured DNA and RNA molecules [8,11]. We recently demonstrated that another viral nucleocapsid protein, HIV-1 NC, can chaperone the circularization of long linear dsDNA via the annealing of short single-stranded overhangs [18]. Therefore, we decided to investigate if HCVcp can perform the same task. This was done by monitoring either: (*i*) λ-DNA with single-stranded overhangs containing 12 nts or (*ii*) T7-DNA with blunt ends, in the absence and presence of low concentrations (≤0.1 μM) of HCVcp (Fig. 4e and f). In the absence of HCVcp, free λ-DNA uniformly adopted extended structures with an average extension of ~ 7 μm. In the presence of HCVcp, we observed small populations of molecules with either half or twice the average extension of single, linear λ-DNA molecules. The molecules having shorter extension values are circular λ-DNA molecules that are formed due to HCVcp-assisted intramolecular annealing of the single-stranded overhangs. The molecules with twice the normal extension values are linear concatemeric λ-DNA structures (e.g., dimers) that arise from HCVcp-assisted intermolecular annealing. To further support this conclusion, we performed similar experiments with T7-DNA, which has blunt ends, and did not observe the formation of circles or concatemers. The fractional abundance of circles and concatemers for λ-DNA in the presence of HCVcp is limited by the unavoidable competition between the chaperone-assisted annealing at low concentrations (≤0.1 μM) of HCVcp and DNA compaction at higher concentrations.

4. Discussion and conclusion

The goal of this study was twofold; to demonstrate how we can study global structural changes in long dsDNA molecules that are individually-confined in solution using a novel nanofluidic device and to use this methodology to understand how the HCVcp interacts with long dsDNA.

The work described above showcases the general utility of nanofluidic devices, particularly our novel dynamic nanofluidic device, for single-molecule investigations of nucleic acid-protein interactions. Compared to other single-molecule methods, nanofluidic channels have several advantages for studying genome-length dsDNA molecules. The use of nanofluidic channels allows molecules to be visualized without any chemical modifications to the ends of the DNA. The ends of linear genomic DNA are important in many areas of biology, e.g., repair of double-stranded breaks in DNA, where our device might prove to be very useful. Furthermore, nanofluidic devices also permit visualization of large, protein-induced structural changes in DNA molecules that are confined in solution using a miniscule stretching force (<1 pN) that is comparable to the forces expected to be present in crowded cellular environments. Finally, the current design associated with our dynamic nanofluidic device makes it possible to dynamically alter the solution conditions, thereby allowing us to iteratively expose the DNA to different proteins.

By exploiting the numerous advantages provided by nanofluidic devices [5], we have been able to investigate how the hepatitis C virus core protein (HCVcp) interacts with genome-length dsDNA. As previously observed for short (<100 nts) DNA and RNA molecules, this positively charged intrinsically disordered viral protein functions primarily as a macromolecular counterion for nucleic acids [8]. In this way, the basic amino acids of the protein screen the repulsive electrostatic interactions between proximal phosphate groups, which allows otherwise extended nucleic acids to more readily adopt compact conformations. Here, we observe that HCVcp-induced compaction: (*i*) preferentially begins at the ends of the linear DNA; (*ii*) occurs in circular DNA that lacks free ends; and (*iii*) is reversible via the addition of Proteinase K. Additionally, the rate of HCVcp-induced compaction of T4-DNA (Fig. S1) increases with increasing protein concentration, suggesting that the extent of compaction is governed by the occupancy of HCVcp on the DNA, which increases at higher concentrations due to the bimolecular nature of this association. However, the full molecular details of the compaction process remain to be explored.

Nevertheless, the global compaction arising from HCVcp binding likely primes nucleic acids (of any length) for further conformational transitions to more charge-dense forms involving, for example, the annealing of unpaired nucleobases. Indeed, we observe that HCVcp can chaperone both inter- and intramolecular annealing of λ-DNA with complementary single-stranded overhangs. Although our investigations focus on dsDNA, it is conceivable that similar principles could also govern the RNA-protein interactions responsible for forming the hepatitis C virus nucleocapsid, as HCVcp-induced RNA compaction and HCVcp-chaperoned RNA conformational transitions are likely essential aspects of the assembly process.

Declaration of competing interest

The authors declare no conflicts of interest.

Acknowledgements

This project was funded by the Swedish Research Council (no. 2015–5062) and Stiftelsen Olle Engqvist Byggmästare. We acknowledge funding from the European Research Council, in the form of an ERC consolidator grant to FW (nanoDNArepair, no. 866238), and the National Institutes of Health, in the form of a COBRE research project grant to EDH (P20GM103638). We acknowledge the group of Tobias Ambjörnsson for the Matlab interface to analyze the nanofluidic data, Zhaowei Liu for guidance with protein purification, Tsegaye Sewunet for preparing the cDNA and Robin Öz for fruitful discussions.

Appendix A. Supplementary data

Supplementary data to this article can be found online at https://doi.org/10.1016/j.bbrc.2020.06.051.

References

[1] K.R. Chaurasiya, T. Paramanathan, M.J. McCauley, M.C. Williams, Biophysical characterization of DNA binding from single molecule force measurements, Phys. Life Rev. 7 (2010) 299–341.
[2] I. De Vlaminck, C. Dekker, Recent advances in magnetic tweezers, Annu. Rev. Biophys. 41 (2012) 453–472.
[3] B.E. Collins, L.F. Ye, D. Duzdevich, E.C. Greene, DNA curtains, in: Methods Cell Biol., Academic Press Inc., 2014, pp. 217–234.
[4] F. Persson, J.O. Tegenfeldt, DNA in nanochannels—directly visualizing genomic information, Chem. Soc. Rev. 39 (2010) 985.
[5] K. Frykholm, L.K. Nyberg, F. Westerlund, Exploring DNA–protein interactions on the single DNA molecule level using nanofluidic tools, Integr. Biol. 9 (2017) 650–661.
[6] C. Zhang, K. Jiang, F. Liu, et al., A nanofluidic device for single molecule studies with in situ control of environmental solution conditions, Lab Chip 13 (2013) 2821.
[7] R. Öz, S. KK, F. Westerlund, A nanofluidic device for real-time visualization of DNA–protein interactions on the single DNA molecule level, Nanoscale 11 (2019) 2071–2078.
[8] E.D. Holmstrom, Z. Liu, D. Nettels, et al., Disordered RNA chaperones can enhance nucleic acid folding via local charge screening, Nat. Commun. 10 (2019) 2453.
[9] T.L.F. de Souza, S.M. Barbosa de Lima, V.L. de Azevedo Braga, et al., Charge neutralization as the major factor for the assembly of nucleocapsid-like particles from C-terminal truncated hepatitis C virus core protein, PeerJ 2016 (2016), e2670.
[10] F. Persson, J. Fritzsche, K.U. Mir, et al., Lipid-based passivation in nanofluidics, Nano Lett. 12 (2012) 2260–2265.
[11] E.D. Holmstrom, D. Nettels, B. Schuler, Conformational plasticity of hepatitis C virus core protein enables RNA-induced formation of nucleocapsid-like particles, J. Mol. Biol. 430 (2018) 2453–2467.
[12] McLauchlan, Properties of the hepatitis C virus core protein: a structural protein that modulates cellular processes, J. Viral Hepat. 7 (2000) 2–14.
[13] E. Santolini, G. Migliaccio, N. La Monica, Biosynthesis and biochemical properties of the hepatitis C virus core protein, J. Virol. 68 (1994) 3631–3641.
[14] K. Frykholm, L.K. Nyberg, E. Lagerstedt, et al., Fast size-determination of intact bacterial plasmids using nanofluidic channels, Lab Chip 15 (2015) 2739–2743.
[15] M. Alizadehheidari, E. Werner, C. Noble, et al., Nanoconfined circular and linear DNA: equilibrium conformations and unfolding kinetics, Macromolecules 48 (2015) 871–878.
[16] J. Krog, M. Alizadehheidari, E. Werner, et al., Stochastic unfolding of nanoconfined DNA: experiments, model and Bayesian analysis, J. Chem. Phys. 149 (2018), 215101.
[17] L.K. Nyberg, S. Quaderi, G. Emilsson, et al., Rapid identification of intact bacterial resistance plasmids via optical mapping of single DNA molecules, Sci. Rep. 6 (2016) 30410.
[18] K. Jiang, N. Humbert, S. KK, T. Lequeu, et al., Annealing of ssDNA and compaction of dsDNA by the HIV-1 nucleocapsid and Gag proteins visualized using nanofluidic channels, Q. Rev. Biophys. 52 (2019) e2.